Journal of Power Sources 195 (2010) 7559–7567

Contents lists available at ScienceDirect

Journal of Power Sources

journal homepage: www.elsevier.com/locate/jpowsour

Gas diffusion layer design focusing on the structure of the contact face with catalyst layer against water flooding in polymer electrolyte fuel cell

Yusuke Hiramitsu*, Kenji Kobayashi, Michio Hori

Fuel Cell Research Center, Daido University, 10-3 Takiharu-cho, Minami-ku, Nagoya, Aichi 457-8530, Japan

ARTICLE INFO

Article history:
Received 23 March 2010
Received in revised form 31 May 2010
Accepted 31 May 2010
Available online 9 June 2010

Keywords:
Polymer electrolyte fuel cell
Water management
Flooding
Gas diffusion layer
Pore structure
Liquid water transport

ABSTRACT

High humidity must be maintained inside polymer electrolyte fuel cells to achieve high ion conductivity. However, water condensation blocks the diffusion of the reaction gas in the gas diffusion layer under water saturation conditions which are produced by the product water. This effect is known as flooding and causes a sudden drop in the cell voltage. Therefore, advanced water management is required in such fuel cells. Internal water management is generally carried out by making adjustments to the gas diffusion layer. This study reports that the extremely highly flood-resistant gas diffusion layer has been developed, based on simple carbon paper. It was experimentally revealed that flooding is controlled by a gas diffusion layer with a smaller pore-structure facing the catalyst layer and it is one of the governing factors for flooding in the gas diffusion layer.

1. Introduction

Polymer electrolyte fuel cells (PEFCs) can generate electricity in the relatively low temperature region from room temperature to 100 °C, and thus have the advantage of fast startup times. From this reason, PEFCs are seen as promising electric power sources for household cogeneration systems and electric vehicles. However, further cost reductions and improvements in efficiency are required before they can be used in practical applications.

One of the most basic requirements is that high power density be achieved. Proton exchange membranes exhibit high proton conductivity under high humidity conditions. Therefore, in order to achieve a high power density, it is necessary to supply fuel and oxidizer under such conditions. However, since water is also a product of the electrochemical reaction, this often leads to saturation water vapor levels and water droplet formation. In addition, for efficient fuel cells it is necessary to control parasitic loss. For this purpose, high gas utilization is thought to be a very effective approach. For the same reason, cell structures that can achieve low pressure loss are also desirable. However, when these conditions are strictly implemented, drainage of condensed water becomes problematic. This leads to instabilities in the cell performance by obstructing oxygen diffusion, resulting in high mass-transfer overpotential. This phenomenon is referred to as flooding. Therefore, water management is extremely important for fuel cells. Ideally, such management should be carried out by the cell components themselves, to avoid the need for complicated external control systems.

In PEFCs, a porous electrode layer is placed between the catalyst layer (CL) and a separator to allow diffusion of the reaction gases to the catalyst. Such a layer is referred to as a gas diffusion layer (GDL) and has a significant effect on water management. Paper or cloth consisting of carbon fiber is usually used for the GDL, because high corrosion resistance and electrical conductivity are required. In general, water management is carried out within the cell components at the polymer electrolyte membrane (PEM), the CL and the gas flow channel in the separator. The GDL should provide high effective gas permeability even when its water content is high or/and should allow efficient water drainage.

A GDL is generally a carbon macroporous layer such as carbon paper or carbon cloth. It is usually treated with a water-repellent substance such as polytetrafluoroethylene (PTFE). For effective water management, the GDL thickness, porosity and hydrophobicity are important for optimizing gas diffusivity and water drainage [1–9].

Alternatively, a microporous layer (MPL), consisting of fine carbon black and PTFE powder, can be coated on the macroporous layer using a wet or dry process. This type of MPL has a remarkable influence on cell performance in water-saturated conditions. The MPL thickness [9], porosity, PTFE ratio and carbon-black properties

* Corresponding author. Tel.: +81 52 612 6144; fax: +81 52 612 6144.
E-mail addresses: hiramitu@daido-it.ac.jp (Y. Hiramitsu), k3kenji@daido-it.ac.jp (K. Kobayashi), hori@daido-it.ac.jp (M. Hori).

0378-7753/$ – see front matter © 2010 Elsevier B.V. All rights reserved.
doi:10.1016/j.jpowsour.2010.05.067

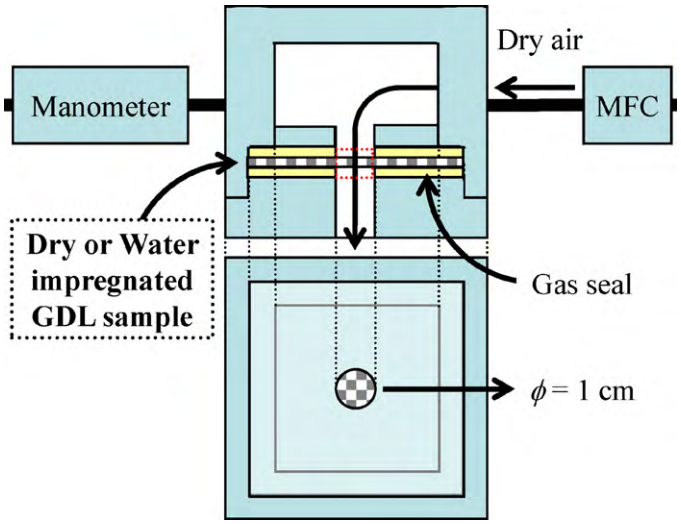

Fig. 1. Experimental set up for measuring the gas permeability and dehydration pressure of a GDL. MFC indicates a mass flow controller.

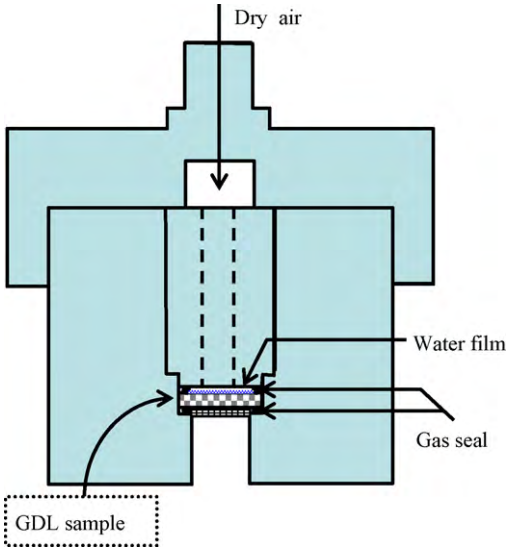

Fig. 2. Experimental apparatus for measuring the water permeance pressure of a GDL.

also have a strong influence on gas diffusivity and water drainage in such GDLs [10–17].

A large number of studies of two phase modeling of flooding in PEFCs have been carried out [18–27]. By modeling the degree of water saturation through the thickness of the GDL, the highest saturation was found at the contact face with the CL, and decreased gradually toward the gas flow channel. The physical properties of the GDL and MPL have a large influence on this water saturation [24–27]. Through theoretical studies, Sinha et al. highlighted the importance of water management at the CL/GDL interface [26,27]. A hydrophilic-hydrophobic hybrid GDL was suggested as a means of achieving a good balance between gas diffusion and drainage of the CL/GDL interfacial water [26–28]. In addition, the flood-proofing properties of carbon cloth are generally better than those of carbon paper. This is thought to be because the large pores between the crossed fibers drain the water accumulating at the CL/GDL interface [29,30]. In a similar approach, the present authors previously reported on the suppression of flooding by punching through-holes in the GDL [7]. The authors also considered the pore structure in the region of the GDL immediately adjacent to the CL, and found that flooding could be greatly reduced by producing a micronized hydrophobic structure in this region [9].

The above methods, however, involve higher costs, because additional complex processes are required to manufacture the GDL. To realize the practical application of fuel cells, cost reductions are desired for all of the materials and processes used to produce them. Cost performance has a high priority, even for critical technologies. Therefore, the practical use of the above techniques is not feasible, and simple manufacturing and easy handling methods are desired for the GDL.

In this study, flood-proofing of carbon paper using a micronizing process was investigated. The basic properties of the resulting GDLs were characterized, and their flooding behavior during power generation was evaluated. In this article, one of the most critical factors governing flooding was clarified. Furthermore, a low-cost, flood-resistant GDL with superior water management was proposed.

Table 1
GDL specifications.

Carbon paper	Thickness (μm)	Bulk density (g cm^{-3})
TGP-H-030	111	0.43
TGP-H-060	200	0.44
WMGDL	114	0.31
×0.6 WMGDL	70	0.29
×2 WMGDL	200	0.40

2. Experimental

2.1. GDL preparation

2.1.1. Specifications of carbon paper for GDL

TGP-H-H030 (H030, Toray Industries, Inc., Japan) and a prototype water-management GDL (WMGDL, Mitsubishi Rayon Co., Ltd., Japan) composed of non-woven carbon paper were used in this study. The thickness and the bulk density of H030 and WMGDL are shown in Table 1. The GDLs which were evaluated as the references are also shown in Table 1.

2.1.2. Hydrophobic treatment

Hydrophobic pretreatment was performed on the GDLs by dipping in a 12 wt% PTFE dispersion (31-JR, DuPont-Mitsui Fluorochemicals Co., Ltd, Japan) and by heating at 350 °C for several minutes in an electric muffle furnace (FUW230PA, Toyo Roshi Kaisha, Ltd., Japan). To evaluate the effect of PTFE loading, the same hydrophobic pretreatment was performed twice for H030.

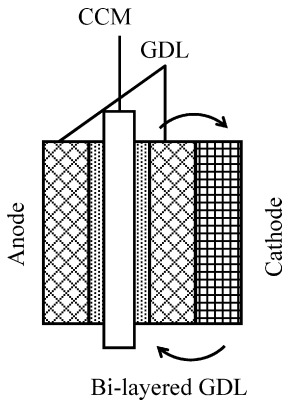

Fig. 3. The MEA structure of bi-layered cathode GDL to evaluate the GDL structure facing CL.

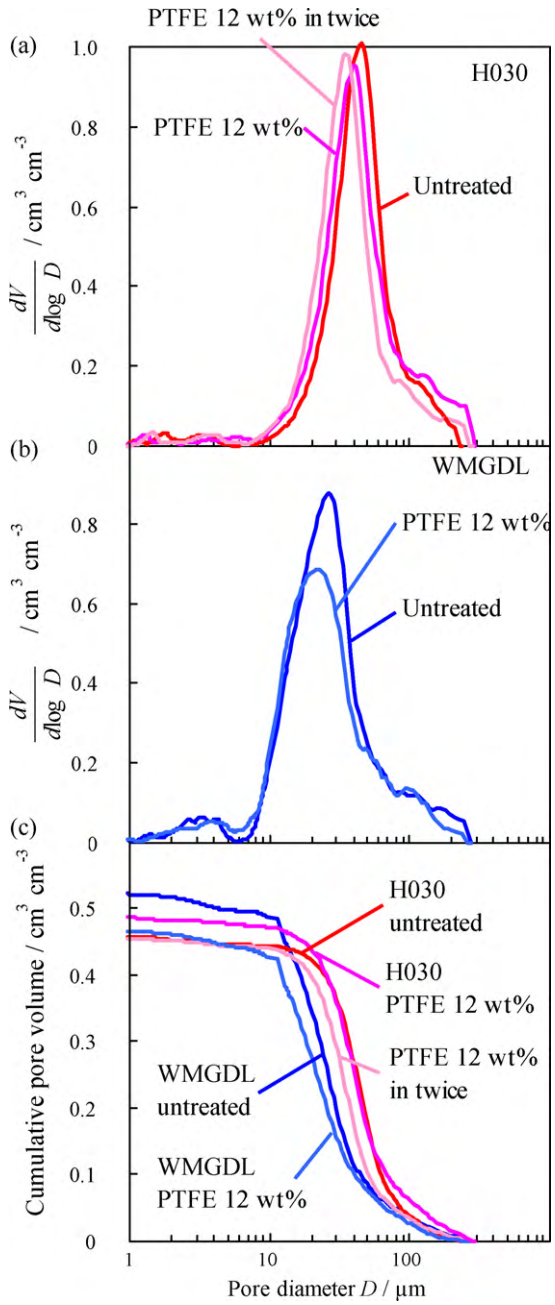

Fig. 4. Pore size distribution of GDL measured by mercury intrusion porosimetry. (a) H030, (b) WMGDL and (c) cumulative pore volume.

2.2. GDL characterization

2.2.1. Porosimetry

Measurement of the pore size distribution was carried out using mercury intrusion porosimetry (Poresizer 9320, Micromeritics Instrument Corp., USA) to characterize the pore structure of the carbon paper consisting of carbon fibers and binder.

2.2.2. Morphology

The state of the binder between the carbon fibers, the adhesion of the PTFE, and the shape of the carbon fibers were observed by scanning electron microscopy (SEM, JSM-6300F, JEOL, Ltd., Japan).

2.2.3. Gas permeability

Fig. 1 shows a schematic of the experimental apparatus used to measure the gas permeability of the GDL. A dry GDL was sandwiched between two PTFE sheets and two aluminum plates, each containing a hole 1 cm in diameter. This was installed in an aluminum case as shown in the figure, such that the interior of the case was separated from the outside atmosphere by only the GDL. A tube connected to a manometer (6349, Testo K. K., Japan) was then attached to the case. The flow rate of air was controlled by a mass flow controller (CMQ-V, Yamatake Corp., Japan). When the gas flowed, the pressure loss due to diffusion through the GDL was measured.

The gas permeability Q was calculated from the measured flow rate V and differential pressure ΔP by Eqs. (1) and (2).

$$R = \frac{\Delta P}{V} \quad (1)$$

$$Q = \frac{T}{RS} \quad (2)$$

where R: airflow resistance, T: thickness of GDL, S: area of GDL, 1 kPa = 102.064 mmAq.

2.2.4. Drainage properties

Measurement of the dehydration pressure was performed as follows. First, the GDL was impregnated by water vacuum impregnation [8,31]. In this process, the GDL was subjected to a vacuum of −96 kPa under water. When air bubbles stopped emerging from the GDL it was returned to atmospheric pressure while still under water. This process was repeated several times and the weight change was measured.

The water-impregnated GDL was installed in the apparatus illustrated in Fig. 1. Under gas flow, the stable internal pressure was quickly measured with a pressure gauge (AP-C40, Keyence corp., Japan) and the procedure described in Section 2.2.3 was carried out. With increasing flow rate, the internal pressure rose. The pressure just before the point when the internal pressure decreased for the first time was defined as the dehydration pressure ΔP_D.

2.2.5. Water permeance pressure

Measurement of the water permeance pressure was performed using a capillary flow porometer (CFP-1200-AEXL, Porous Materials Inc., USA) to evaluate the hydrophobicity and the influence on water transport of the GDL pore structure. Fig. 2 shows a schematic diagram of the experimental apparatus to measure the water permeance pressure. The diameter of the measured region of the GDL was 1.3 cm. Water was dropped onto the surface of a dry GDL until a film with a thickness of several mm was produced. The air pressure on the water film was then slowly raised. The water permeance pressure ΔP_p was defined as the pressure when the air flow rate through the GDL showed a sudden increase.

2.3. Power generation

2.3.1. Polarization measurements

As mentioned earlier, a power generation test was carried out on a single cell to examine the flooding behavior of the GDL.

A catalyst-coated membrane (CCM) was used in this test (PRIMEA series, Japan Gore-tex Inc., Japan). The CCM contained a CL with a Pt loading of 0.3 mg cm^{-2} and a PEM with a thickness of 30 μm. The CCM was sandwiched between two sheets of GDL to produce a membrane electrode assembly (MEA). The active area of the MEA electrode was 30 × 150 mm^2. The MEA was tightly fastened together using two carbon separators with flow fields (Nippon Carbon Co., Ltd., Japan). Sixteen straight 1-mm-wide channels were machined into the separator, measuring 150 mm in length, and the ribs separating the channels were 1 mm wide. The

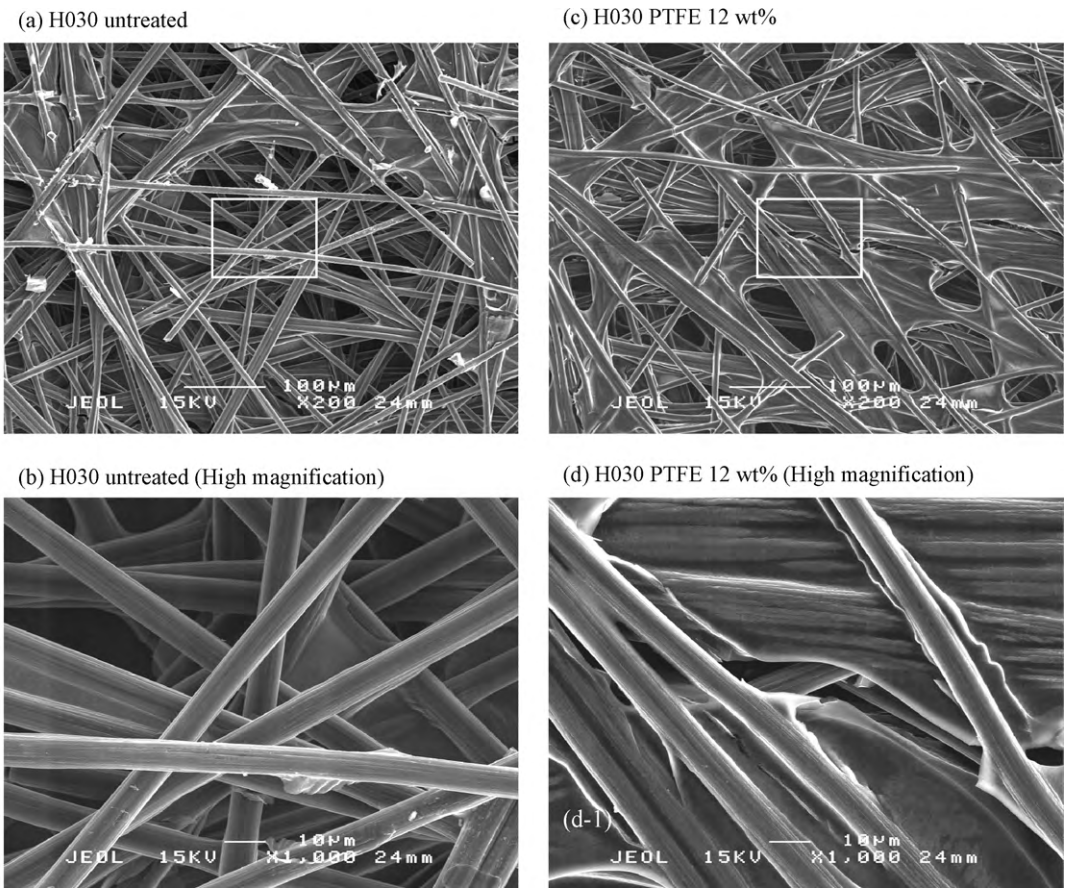

Fig. 5. SEM images of H030.

depths of the channels were 0.5 mm at the cathode and 0.4 mm at the anode. The fuel and oxidant were supplied using a counter-flow configuration through alternating channels.

A fuel cell test stand (Kojima Instruments Inc., Japan) was used to evaluate the performance of the fuel cell. Polarization curves for the cell were measured such that the load current with an electric load (PLZ664WA, Kikusui Electronics Corp., Japan) was increased at the rate of 5 A min^{-1} to a current density of 1.50 A cm^{-2} with constant gas utilization. The gas utilization of the fuel and the oxidant was 70% or 40%. The operating pressure was atmospheric pressure. The cell temperature was 75 °C. The humidification temperature was varied from 40 to 85 °C. The humidification level of the oxidant was the same as that of the fuel.

The limiting current density was estimated from the polarization curve. This is one index of the gas diffusivity of the MEA. Here, it is defined as the current density at a cell voltage of 0 V, and is determined by linear extrapolation of the polarization curve.

2.3.2. Polarization measurement with different GDL structure at CL/GDL interface

A power generation test was performed to evaluate the influence of the structure of the CL/GDL interface on flooding. The configuration of the MEA is shown in Fig. 3. On the cathode side, the GDL had a bi-layer structure using the combinations of WMGDL and H030 listed in Table 2. For the saturated condition, the cell and the humidification temperature was set to 75 °C and 80 °C, respectively. For the non-saturated condition, the cell and the humidification temperature was set at 80 °C and 70 °C, respectively. The fuel and oxidant gas utilization was 70%.

3. Results

3.1. GDL characterization

3.1.1. Porosity

Fig. 4 shows the pore size distribution and cumulative pore volume of each GDL measured by mercury intrusion porosimetry. As shown in Fig. 4(a) and (b), by comparing the distributions, it was found that the pores in WMGDL were both smaller and more numerous than those in H030. As shown in Fig. 4(c), by comparing the pore volume, it was found that the volume of WMGDL mainly consisted of the small pores and the volume of H030 mainly consisted of the large pores, clearly.

Table 3 shows the pore-structure parameters calculated from the pore size distributions. The porosity of WMGDL was slightly lower than that of H030. In addition, the measured porosity of H030 was found to be lower than the value published by the manufacturer. It is thought that this was due to the presence of surface

Table 2
Combinations of bi-layered GDL on cathode to evaluate the GDL structure facing CL.

GDL settings		WM/WM	WM/030	030/WM	030/030
Cathode	Channel side	WMGDL	H030	WMGDL	H030
	CL side	WMGDL	WMGDL	H030	H030

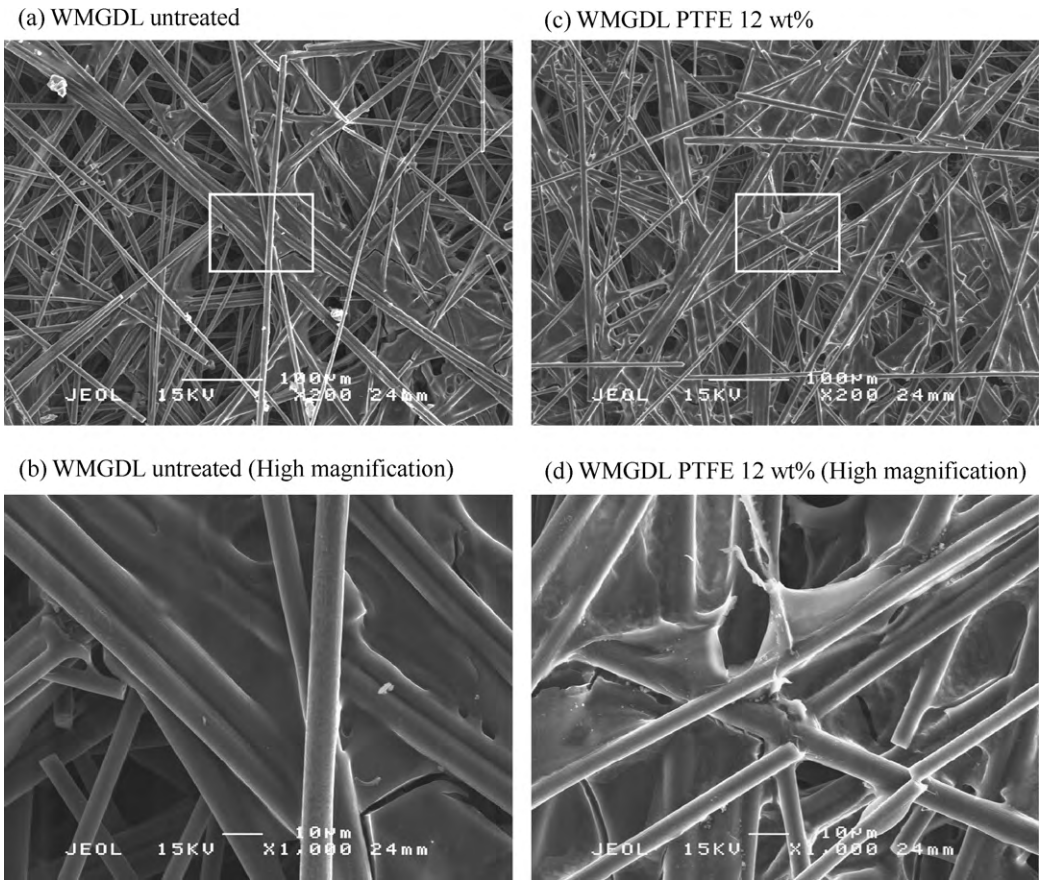

Fig. 6. SEM images of WMGDL.

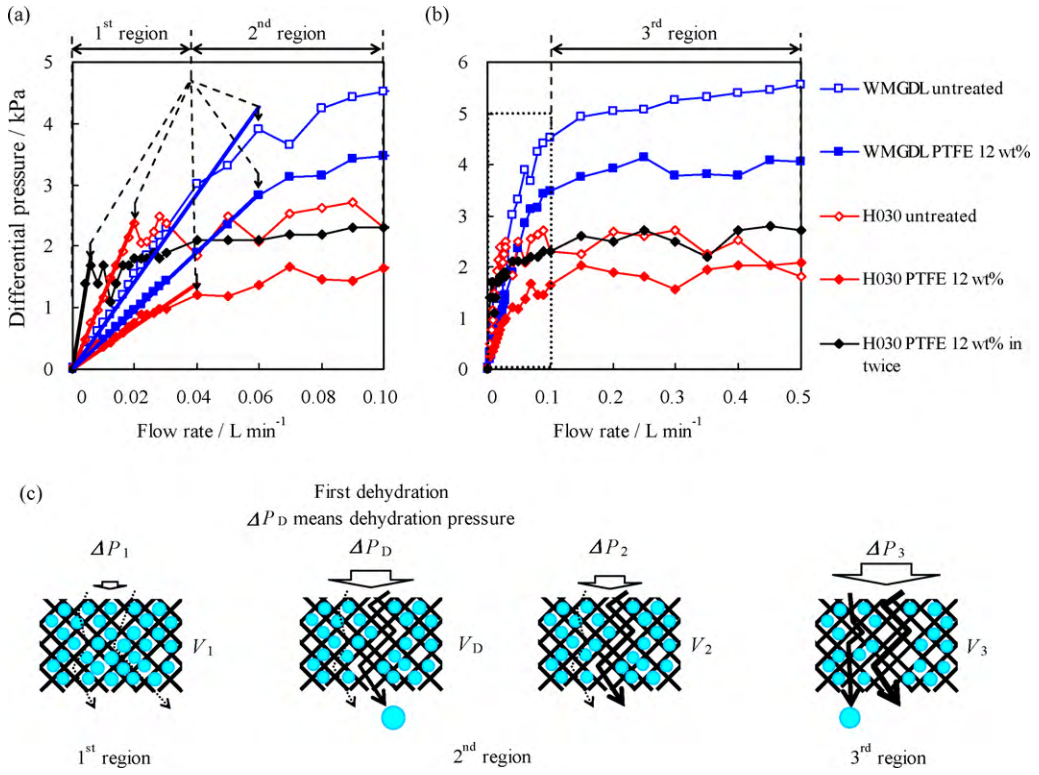

Fig. 7. Relationship between flow rate and differential pressure with water-impregnated GDL. (a) Close up of the 1st proportional region until the first dehydration and 2nd region. (b) 3rd dehydrating region in whole region. (c) Schematics of each region. These schematics are the portion shown in Fig. 1 with the dashed line.

roughness that allowed the mercury to slightly penetrate the material even in the absence of pressure.

The surface area of WMGDL was larger than that of H030. Thus, using the same water-proofing treatment, the PTFE adhered to more WMGDL than H030.

The GDL pore structure became micronized due to adhesion of PTFE. Although the average pore diameter in H030 decreased following two successive water-proofing treatments, it still remainder larger than that in WMGDL. This shows that it is difficult to effectively micronize the pore structure by PTFE adhesion.

3.1.2. Morphology

Figs. 5 and 6 show SEM images of H030 and WMGDL, respectively. Both GDLs were made of carbon paper, and so their basic structure was similar. WMGDL was found to contain more fibers than H030, and appeared to have a finer pore structure. The diameter of the carbon fibers in H030 was measured to be approximately 10 μm. On the other hand, in WMGDL, two different fiber diameters of approximately 10 μm and 8 μm were observed.

Figs. 5(c) and (d) and Fig. 6(c) and (d) show SEM images of water-proofed H030 and WMGDL, respectively. It can be seen that the pore structure was dramatically changed by the water-proofing treatment. The PTFE can be seen clinging to the carbon fibers and binder, thereby reducing the pore size.

3.1.3. Gas permeability

Table 4 shows the gas permeability along the thickness direction of dry GDL measured by the apparatus illustrated in Fig. 1. The gas permeability was smaller in WMGDL than in H030. This was consistent with the measured pore diameters. In addition, the gas permeability decreased following the water-proofing treatment.

3.1.4. Drainage properties

Water-impregnated GDLs were placed in the apparatus shown in Fig. 1, and the relationship between the flow rate and the differential pressure was measured. The water saturations in H030, water-proofed H030, WMGDL and water-proofed WMGDL were found to be 0.83, 0.54, 0.73 and 0.56, respectively.

Fig. 7 shows the relationship between the flow rate and differential pressure. These curves seemed to be divided into three regions.

The first region was from a flow rate of zero to that which caused the differential pressure to decrease for the first time as shown in Fig. 7(a). Up to this point, the differential pressure increased in proportion to the flow rate. This indicates that gas permeability was observed under wet conditions. A comparison of the gas permeability in dry and wet conditions is shown in Table 4.

In the second region, a sudden sharp drop occurred in the differential pressure. This indicated that a rapid localized increase in void space occurred due to dehydration of the GDL. This differential pressure was defined as the dehydration pressure ΔP_D. The differential pressure rose again following this, possibly because the newly formed empty voids became obstructed again by nearby regions of water.

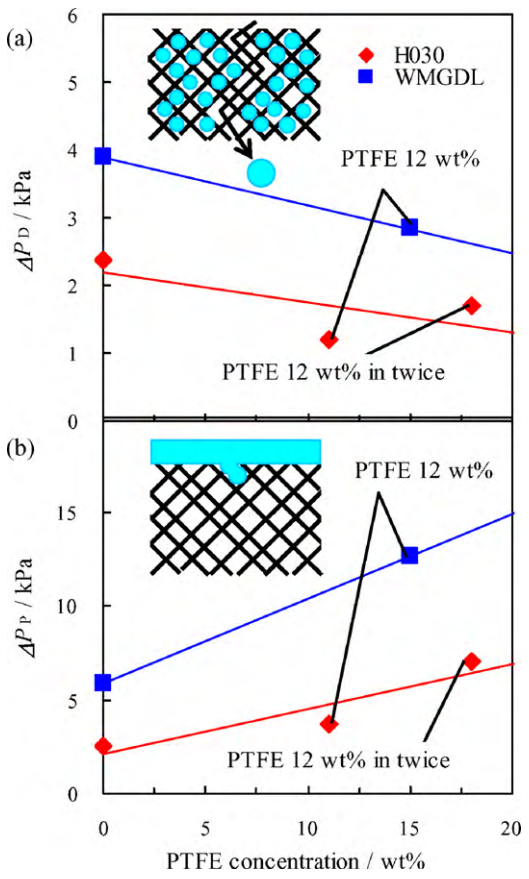

Fig. 8. Relationships between (a) PTFE concentration and dehydration pressure. The inset shows the schematic of dehydration pressure. (b) PTFE concentration and water permeance pressure. The inset shows the schematic of permeance pressure.

In the third region, the differential pressure again increased with flow rate, but more moderately than in the first region, and eventually became constant as shown in Fig. 7(b). It is believed that continuous dehydration and evaporation were occurring in the GDL in this region.

Fig. 8(a) shows the relationship between the PTFE concentration and the dehydration pressure. The dehydration pressure was smaller for the GDL with the larger pore size. Furthermore, it was also smaller for the water-proofed GDLs. These results show that water was easily released from those GDLs.

3.1.5. Water permeance pressure

Fig. 8(b) shows the results for the water permeance pressure ΔP_p. The water permeance pressure increased with PTFE concentration for both H030 and WMGDL. In addition, it was smaller for H030 than for WMLGDL. Since the pore size in H030 was larger than that in WMLGDL, as shown in Fig. 4 and Table 3, this indicates that water moves through the GDL by capillary action.

Table 3
Pore-structure parameters calculated from distributions shown in Fig. 4.

Carbon paper	PTFE concentration (wt%)	Mean pore diameter d (μm)	Peak pore diameter d_{peak} (μm)	Porosity ($cm^3\ cm^{-3}$)	Specific surface area ($m^2\ cm^{-3}$)
TGP-H-030	0	23	45	0.46	0.080
	11	20	40	0.49	0.095
	18	11	35	0.46	0.166
WMGDL	0	14	26	0.53	0.153
	15	11	24	0.47	0.183

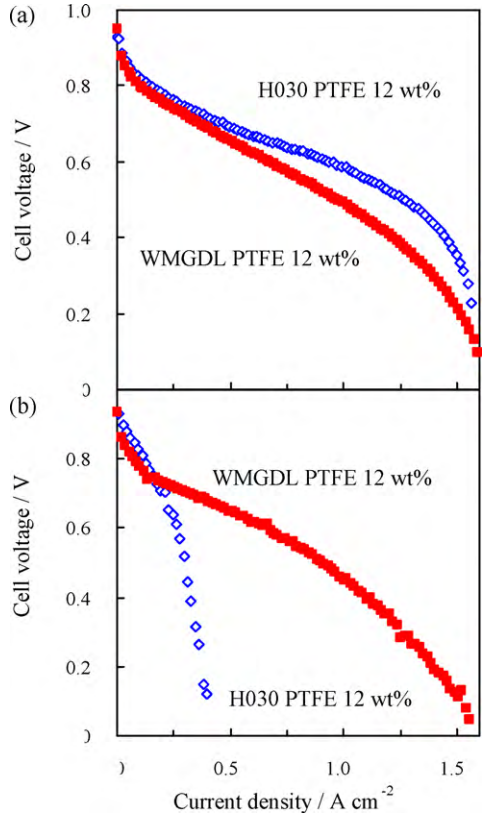

Fig. 9. Polarization curves. (a) Cell temperature was 75 °C, humidification temperature was 60 °C, fuel utilization was 70% and air utilization was 40%. (b) Cell temperature was 75 °C, humidification temperature was 75 °C, fuel utilization was 70% and air utilization was 70%.

3.2. Power generation test

3.2.1. Polarization

Fig. 9(a) shows typical polarization curves under low humidification at 64%RH and low gas utilization conditions, and Fig. 9(b) shows those under saturated humidification and high gas utilization conditions. Both H030 and WMGDL exhibited high performance for all current densities when the humidification and gas utilization were low. On the other hand, for high humidification and gas utilization, H030 exhibited a significant decrease in cell performance at high current density, whereas WMGDL did not. This indicates that H030 caused flooding but WMGDL did not.

Furthermore, the humidification temperature dependence of the limiting current density is shown in Fig. 10. The flood-proof characteristics of WMGDL are seen to have been improved by the water-proofing treatment. In addition, the limiting current density did not decrease for WMGDL, even when the vapor pressure exceeded the saturating condition during high gas utilization. In contrast, the flood-proof characteristics of H030 did not improve following the same treatment. In fact, water-proofed H030 caused a remarkable amount of flooding.

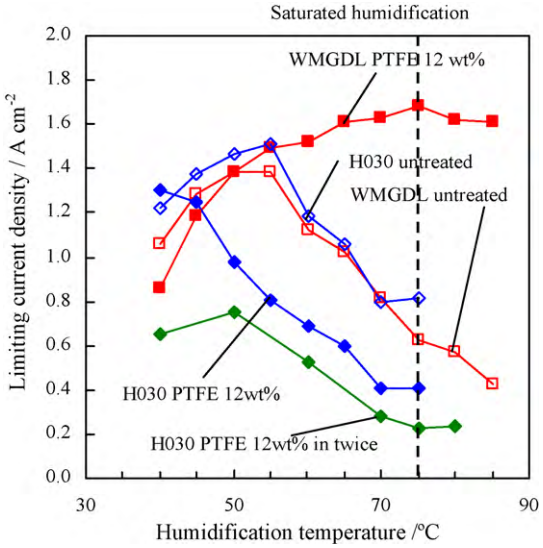

Fig. 10. Humidification temperature dependence of the limiting current density.

3.2.2. Polarizations with different GDL structure at CL/GDL interface

Fig. 11 shows the results of power generation tests for single cells containing the MEAs shown in Fig. 3. The combinations used in the bi-layered GDL are shown in Table 2. It was found that the higher cell voltages were produced when WMGDL was placed on the CL side in the cathode.

4. Discussion

It is necessary to clarify the governing factor among some flooding factors for designing the outstanding water-management GDL. Firstly, hydrophobicity is treated on GDL to repel water. The relationship between the hydrophobic treatment method and/or strength, and flooding has been investigated in previous study [3]. On the other hand, since hydrophobicity reduces the water permeability, it is not the only factor which governs flooding [25,27]. Secondly, the GDL structure also influences the flood-proof characteristics. When the same hydrophobic treatment is performed, the GDL pore structure affects the water transport property and water distribution. The water transport property of GDL which relates to the drain of the condensed water from CL to flow channel might be

Table 4
Gas permeability of GDL.

Carbon paper	PTFE concentration (wt%)	Air permeability ($ml\,cm^{-2}\,h^{-1}\,mmAq^{-1}$)	Air permeability (water-impregnated condition) ($ml\,cm^{-2}\,h^{-1}\,mmAq^{-1}$)
		Through plane	
TGP-H-030	0	23,083	6.22
	11	21,619	14.28
	18	15,925	0.02
WMGDL	0	11,529	10.14
	15	10,458	15.16
TGP-H-060 (i.e. ×2 TGP-H-030)	14	8015	5.41
×2 WMGDL	17	3152	0.02
×0.6 WMGDL	16	18,712	2.95

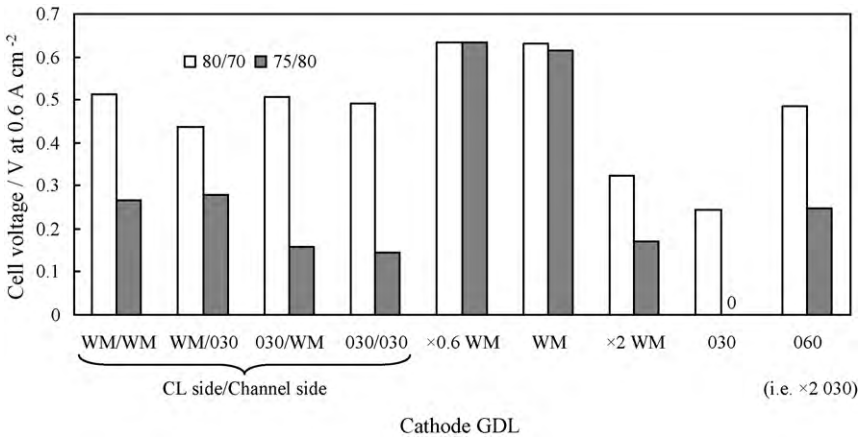

Fig. 11. Cell voltage at current density of 0.6 A cm^{-2} with bi-layered GDL on cathode. The different cathode GDL combinations are shown in Table 2. ×0.6 WMGDL, ×2 WMGDL, H060 are 0.6 times, twice the thickness of WMGDL and twice the thickness of H030, respectively, which are shown as the references.

an extremely important physical property. This is estimated from the equation of the capillary pressure. Water transport in a single pore can be expressed by Eq. (3).

$$P = \frac{-4\gamma \cos\theta}{d} \tag{3}$$

where P: capillary pressure, γ: interfacial surface tension of water, θ: contact angle, d: pore diameter.

The hydrophilic GDL absorbs water, and is saturated, and its gas diffusivity decreases. Therefore, the contact angle of GDL must be 90° or more, and when pore diameter is large, the water transport property is high in that condition.

For accelerating GDL development, authors have been evaluating the physical properties of GDL, and have examined the governing property which can evaluate the flood-proof characteristics of GDL, elementally. As a fundamental study, the relationship between the cell polarization and the gas diffusivity, the water permeability, the water drainage as physical properties of 20 or more kinds of GDL has been investigated. As a result, clear negative correlation was seen between limiting current density and dehydration pressure as water drainage [7]. Therefore, the situation of water drainage would be similar to that of power generation.

In these experiments, water-proofed H030 consisting of larger pore structure than water-proofed WMGDL as shown in Sections 3.1.1 and 3.1.2 had higher gas permeability as shown in Section 3.1.3, higher water permeability as shown in Section 3.1.5 and lower dehydration pressure as shown in Section 3.1.4. Those results show that water-proofed H030 has better mass transport properties. Nevertheless, flooding was occurred significantly with water-proofed H030 as shown in Section 3.2.1.

Thus, the mass transport properties of WMGDL are less than H030. However, as shown in Section 3.2.1, the stable high performance without flooding was maintained under the saturated humidification and high gas utilization at 70%. The relationship between GDL structure and flooding, in a previous report, the authors revealed that flooding could be controlled by H030 micronized on the side facing the CL by a small amount of water-proofed carbon particles [9].

Then, the power generation test with bi-layer GDL was examined in order to obtain evidence that the structure of carbon paper that had a minute pore structure like WMGDL controlled the flooding at CL/GDL interface.

The comparison of polarization with bi-layer GDL on cathode, which is shown in Fig. 11 in Section 3.2.2 demonstrates that the region of the GDL immediately adjacent to the CL governs flooding in the GDL and the smaller pore-structure facing CL is effective against flooding.

This concept is illustrated in Fig. 12. It is thought the CL containing ionomer which generates water gets wet easily compared with water-proofed GDL. Then, it is easy to accumulate water between a hydrophobic GDL and such a CL with a higher water affinity than the GDL according to Eq. (3). As shown in Fig. 12(c) and (d), when the pores in GDL at the side of CL/GDL interface are larger, the larger water layer will be formed over CL surface because of this hydrophobicity difference between CL and GDL, and this water layer would then block gas diffusion. However, as shown in

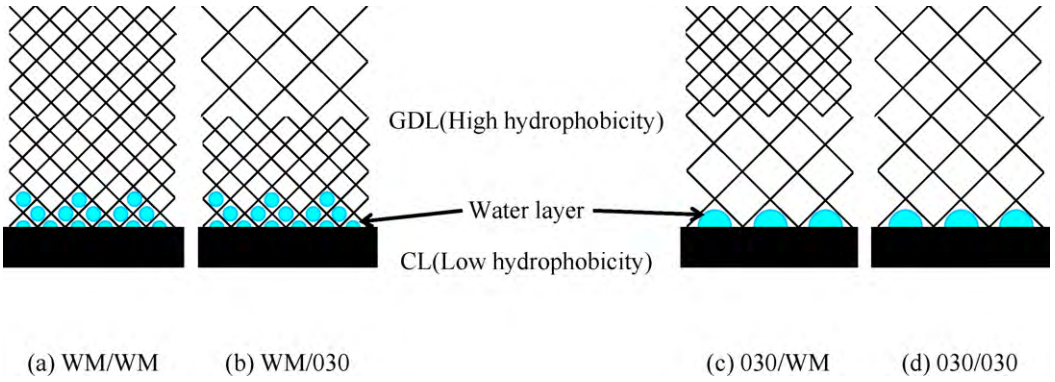

Fig. 12. Schematic images of flooding in bi-layered GDL on cathode.

Fig. 12(a) and (b), the water will become highly dispersed in the presence of small pores, and the gas can effectively diffuse from the pores, and flooding would be controlled.

In addition, the influence of the GDL structure facing the gas channel was relatively small in this examination.

From another viewpoint, even if the smaller pore-structure GDL is effective against flooding at CL/GDL interface, the mass transport characteristics are lower. In this regard, the GDL thickness is expected to be an important parameter affecting the flood-proof characteristics. Then, thickness dependence was examined as shown in Fig. 11. With ×0.6 WMGDL, the similar cell performance was obtained. This suggests that the influence of the gas diffusivity and/or water drainage under ribs is small even at this thinness with this smaller pore-structure. In addition to the effect of highly-dispersing water layer at CL/GDL interface, it is presumed that improvements of the gas and water transport properties through the thickness direction by thinning can contribute to control flooding.

On the other hand, the cell performance fell greatly with ×2 WMGDL as shown in Fig. 11. The cell performance fell also in the milder low humidification conditions for flooding. In thick smaller pore-structure GDL, it is shown that the gas diffusivity fell due to increase the amount of accumulated water in GDL according to decreasing water transport property. This suggests that water transport property of GDL governs flooding, if it falls too much like this case. Therefore, it can be said that the balance between micronizing structure facing CL/GDL interface and thinness is the key.

In addition, the flooding with H030/H030 and H060 were smaller than that of H030 as shown in Fig. 11.

The influence of accumulated water under ribs may be suppressed because water and gas would be transported efficiently from under ribs to gas channels with H030/H030 and H060 which are thick compared with H030.

In order to understand these, it is necessary to know the gas permeability of GDL in wet. The gas permeability of the GDL which was impregnated by water vacuum impregnation as shown in Table 4 is not correlated with polarizations. It is estimated that this element examination is not reproducing the water saturation and a contact interface between CL and GDL under power generation.

In order to clarify the above-mentioned presumption, visualization experiments using neutron radiography or X-ray CT should be performed considering the structure of GDL as an experimental parameter. These in situ observations would be expected to provide much more detailed information on the relationship between flooding and the GDL structure facing the CL and water transport property [32–34].

5. Conclusion

An extremely highly flood-resistant GDL has been developed, based on simple carbon paper. It was experimentally shown that flooding was inhibited by a GDL with a smaller pore structure. In addition, it was found that the GDL structure directly facing the CL is one of the governing factors for flooding in the GDL.

Acknowledgements

The authors express their special thanks to all those who assisted in the writing of this article. This research was performed under a grant from the Water Management Project from the New Energy and Industrial Technology Development Organization (NEDO) for strategic technical development for the practical realization of PEFCs. The water-management GDL was prototyped by Mitsubishi Rayon Co., Ltd., Japan in the collaborative study for the Water Management Project.

References

[1] N. Holmstrom, J. Ihonen, A. Lundblad, G. Lindbergh, Fuel Cells 7 (2007) 306–313.
[2] M.V. Williams, E. Begg, L. Bonville, H.R. Kunz, J.M. Fenton, Journal of The Electrochemical Society 151 (2004) A1173–A1180.
[3] G. Lin, T.V. Nguyen, Journal of The Electrochemical Society 152 (2005) A1942–A1948.
[4] J. Ihonen, M. Mikkola, G. Lindbergh, Journal of the Electrochemical Society 151 (2004) A1152–A1161.
[5] K.F. Chiu, K.W. Wang, Surface & Coatings Technology 202 (2007) 1231–1235.
[6] H. Yamada, T. Hatanaka, H. Murata, Y. Morimoto, Journal of the Electrochemical Society 153 (2006) A1748–A1754.
[7] Y. Hiramitsu, K. Hirose, K. Kobayashi, M. Hori, Transactions of Materials Research Society of Japan 33 (2008) 1113–1117.
[8] Y. Hiramitsu, K. Okada, K. Kobayashi, M. Hori, Fiber Preprints, Japan 63 (2008) 192.
[9] Y. Hiramitsu, H. Sato, M. Hori, Journal of Power Sources 195 (2010) 5543–5549.
[10] A.Z. Weber, J. Newman, Journal of the Electrochemical Society 152 (2005) A677–A688.
[11] H.K. Atiyeh, K. Karan, B. Peppley, A. Phoenix, E. Halliop, J. Pharoah, Journal of Power Sources 170 (2007) 111–121.
[12] E. Antolini, R.R. Passos, E.A. Ticianelli, Journal of Applied Electrochemistry 32 (2002) 383–388.
[13] J.M. Song, S.Y. Cha, W.M. Lee, Journal of Power Sources 94 (2001) 78–84.
[14] Z. Qi, A. Kaufman, Journal of Power Sources 109 (2002) 38–46.
[15] J. Yu, Y. Yoshikawa, T. Matsuura, M.N. Islam, M. Hori, Electrochemical and Solid-State Letters 8 (2005) A152–A155.
[16] J. Yu, M.N. Islam, T. Matsuura, M. Tamano, Y. Hayashi, M. Hori, Electrochemical and Solid-State Letters 8 (2005) A320–A323.
[17] X.L. Wang, H.M. Zhang, J.L. Zhang, H.F. Xu, Z.Q. Tian, J. Chen, H.X. Zhong, Y.M. Liang, B.L. Yi, Electrochimica Acta 51 (2006) 4909–4915.
[18] G. Lin, T.V. Nguyen, Journal of the Electrochemical Society 153 (2006) A372–A382.
[19] U. Pasaogullari, C.Y. Wang, Journal of the Electrochemical Society 151 (2004) A399–A406.
[20] U. Pasaogullari, P.P. Mukherjee, C.Y. Wang, K.S. Chen, Journal of the Electrochemical Society 154 (2007) B823–B834.
[21] P.P. Mukherjee, C.Y. Wang, Journal of The Electrochemical Society 154 (2007) B419–B426.
[22] V.P. Schulz, J. Becker, A. Wiegmann, P.P. Mukherjee, C.Y. Wang, Journal of the Electrochemical Society 154 (2007) B419–B426.
[23] G. Inoue, T. Yoshimoto, Y. Matsukuma, M. Minemoto, Journal of Power Sources 175 (2008) 145–158.
[24] U. Pasaogullari, C.Y. Wang, K.S. Chen, Journal of the Electrochemical Society 152 (2005) A1574–A1582.
[25] U. Pasaogullari, C.Y. Wang, Electrochimica Acta 49 (2004) 4359–4369.
[26] P.K. Sinha, C.Y. Wang, Electrochimica Acta 52 (2007) 7936–7945.
[27] P.K. Sinha, C.Y. Wang, Chemical Engineering Science 63 (2008) 1081–1091.
[28] N. Yasuda, S. Takagi, H. Nishiguchi, H. Fukumoto, S. Yoshioka, T. Murahashi, Fiber Preprints, Japan 64 (2009) 34.
[29] Y. Wang, C.Y. Wang, K.S. Chen, Electrochimica Acta 52 (2007) 3965–3975.
[30] D. Spernjak, A.K. Prasad, S.G. Advani, Journal of Power Sources 170 (2007) 334–344.
[31] S. Wang, Y. Utaka, Y. Tasaki, Journal of the Japan Society of Mechanical Engineering B 71 (2005) 1647–1654.
[32] C. Hartnig, I. Manke, R. Kuhn, N. Kardjilov, J. Banhart, W. Lehnert, Applied Physics Letters 92 (2008) 134106.
[33] P. Krüger, R. Kuhn, C. Harting, I. Manke, Meeting Abstract Electrochemical Society 902 (2009) 850.
[34] T. Swamy, E.C. Kumbur, M.M. Mench, Journal of the Electrochemical Society 157 (2010) B77–B85.